ORNL/TM-2024/3561

Fabrication and Testing of Micro Flux Monitors in the High Flux Isotope Reactor

Padhraic. L. Mulligan
David C. Glasgow
Benjamin A. La Riviere

September 2024

OAK RIDGE National Laboratory

ORNL IS MANAGED BY UT-BATTELLE LLC FOR THE US DEPARTMENT OF ENERGY

ORNL/TM-2024/3561

Nuclear Energy and Fuel Cycle Division
Chemical Sciences Division
Electrification and Energy Infrastructure Division

FABRICATION AND TESTING OF MICRO FLUX MONITORS IN THE HIGH FLUX ISOTOPE REACTOR

Padhraic. L. Mulligan
David C. Glasgow
Benjamin A. La Riviere

September 2024

Prepared by
OAK RIDGE NATIONAL LABORATORY
Oak Ridge, TN 37831
managed by
UT-BATTELLE LLC
for the
US DEPARTMENT OF ENERGY
under contract DE-AC05-00OR22725

TABLE OF CONTENTS

LIST OF FIGURES

LIST OF TABLES

ABSTRACT

Neutron dosimetry is a critical technique to measure the neutron flux, fluence, and energy spectrum of nuclear reactors and can be used to indicate fuel reloading, high-power operations, or changes in cycle length. This work presents results of a novel device named the micro flux monitor, which is a miniaturized neutron dosimeter made from small quantities (100s of nanograms) of Ti, Al, Ni, and Au metals deposited on Si and high-purity fused silica substrates using standard semiconductor fabrication techniques. Approximately 1,250 of these devices were produced, and 40 were irradiated in the pneumatic tube facility of the Neutron Activation Analysis Laboratory at the High Flux Isotope Reactor. Testing demonstrated that dosimeter metals can be deposited predictably and repeatedly in multiple geometries, including as quick response (QR) codes. Neutron flux measurements with these devices were within 3% of measurements made using standard flux monitors, demonstrating the efficacy of these devices. Devices were also tested at 500°C under a N_2 atmosphere and showed minimal degradation, suggesting they could be deployed for neutron dosimetry measurements in high-temperature advanced reactors.

1. INTRODUCTION

Neutron fluence and fluence rate measurements are critical to understanding the operational characteristics of nuclear reactors. These measurements are particularly relevant for reactor safeguards purposes, as they can indicate fuel reloading, high-power operations, or changes in cycle length. Neutron fluence measurements are typically performed using the well-established method of neutron dosimetry [1], which functions by placing known masses of high-purity materials in a neutron field and measuring the reaction products following irradiation. The most common materials selected for neutron dosimetry produce delayed gamma-emitting isotopes that can be measured using a high-purity germanium (HPGe) detector. Many ASTM standards exist for selecting appropriate dosimeter materials [2–5], best practices for performing the technique [6, 7], and detector calibration and analysis guidance [8]. Neutron energy spectra can also be determined [9] from dosimetry measurements using standard spectrum adjustment codes such as STAYSL PNNL [10] and SAND-II [11]. Generally, neutron dosimeter materials are in the form of small wires or foils with masses ranging from 1–1,000 mg to minimize flux perturbation, neutron self-shielding, and gamma self-absorption. However, even the smallest foils or wires must account for these attenuation mechanisms and can become highly radioactive (>1 mCi) despite their small mass.

The work in this report describes results of a novel approach to neutron fluence measurements that uses thin film (tens to hundreds of nanometers) and small mass (hundreds to thousands of nanograms) dosimeter materials deposited on a substrate using standard semiconductor fabrication processes. The concept for these devices, named *micro flux monitors* (MFMs), is described in a previous report [12] that outlines the benefits of these devices. These benefits include the ability to colocate multiple dosimeter materials on a single device for streamlined analysis, low residual activity for reduced detector dead time and minimal personnel dose, scalability of material mass for specific applications and conditions, reproducibility for performing redundant measurements, and several other advantages. That report describes the down selection of 4 dosimeter materials from 21 suitable candidates for prototype testing and development of a modeling framework for sizing these materials to investigate their efficacy in performing dosimetry measurements.

MFM devices made from Ti, Al, Ni, and Au were created in 10 different geometries, in 2 different orientations (stacked or coplanar), on 3 different substrate materials in the Center for Nanophase Materials Science cleanroom facility. Forty of these devices were irradiated in the pneumatic tube (PT) facility of the Neutron Activation Analysis (NAA) Laboratory at the High Flux Isotope Reactor (HFIR) [13]. HPGe detectors were used to measure the decay gamma spectra from the devices and were compared with standard flux monitors irradiated on the same day. MFM devices showed a highly linear correlation between dosimeter metal surface area and radioactivity and produced repeatable activities between similar devices. The MFM devices also well matched the activity of ^{198}Au, normalized to mass, in standard flux monitors but with only a fraction of the total radioactivity. Neutron flux measurements with these devices were also within 3% of measurements made with the standard flux monitors. Finally, high-temperature furnace testing was performed under an N_2 atmosphere at 500°C for 64 h on each type of MFM device. Results showed devices coated with a 20 nm layer of Al_2O_3 had minimal changes, while uncoated and metal stacked devices appeared to react with N_2 or form alloys with the other metals. The following provides details of the MFM device fabrication process, reactor and high-temperature testing, and suggestions for future development.

2. DEVICE FABRICATION

MFM devices were fabricated on three types of substrate materials; the details of each are listed in Table 1. Although SiC was originally proposed as the substrate material for this work, Si and high-purity fused silica (HPFS) were found to be much less expensive and readily available alternatives for prototype

fabrication. Two thicknesses of Si were used to investigate whether a thinner substrate would produce lower residual radioactivity following irradiation. HPFS was also investigated to determine whether the lower Si content would produce lower background.

Table 1. 100 mm substrates used for MFM device fabrication

Wafer Material	Wafer Thickness (µm)	Resistivity	Dopants
N-type Si	525	0.008–0.02 Ω-cm	Sb
Undoped Si	300	<20 kΩ-cm	—
High-purity fused silica	500	N/A	—

Five photomasks were designed for patterning MFM devices onto 100 mm wafers, as shown in Figure 1. Separate masks were designed for each of the four MFM metals and contained four differently sized circular device patterns, four differently sized rectangular patterns, and one quick response (QR) code, spread across the entire wafer. Circular and rectangular patterns were designed with equal areas for each size. Dispersing the patterns was intended to capture any differences in metal film thickness between the center and edge of the wafer, which can sometimes occur in electron beam deposition. A fifth photomask was used to pattern individual device serial numbers and dicing guidelines for identification and wafer cutting, respectively. Several square "NAA" patterns were also deposited for each metal. These patterns were intended to be isolated samples of each deposited material for investigation of impurities using NAA.

Wafers were cleaned using a standard RCA clean process before metallization. Photoresist was applied to wafers using MicroPrime P20 hexamethyldisilazane adhesion promoter (Shin-Etsu Microsci, Phoenix, AZ) followed by NFR 016D2–55cP negative photoresist (JSR Micro Inc., Sunnyvale, CA) spin coated at 3,000 rpm for 45 s and a 90 s softbake at 90°C. Wafers were patterned using the previously mentioned custom soda lime photomasks in a Suss MA6 alignment tool (exposure dose of 50 mJ/cm^2), followed by an overbake at 115°C for 90 s. Wafers were developed in tetramethylammonium hydroxide using a programmable spin developer, followed by deionized water cleaning in a Rhetech spin rinser, and a 1 min oxygen plasma descum.

Photopatterned wafers were loaded into a dual-gun electron beam evaporation chamber for deposition of dosimeter materials. Four wafers were secured to an orbiting plate (see Figure 2) and loaded into the e-beam vacuum chamber. Metal layers for coplanar MFM devices were deposited in five separate deposition steps, with nominal thicknesses listed in Table 2. Following deposition, the wafers underwent liftoff in either a 70°C N-methylpyrrolidone (NMP) bath for 30 min or in an acetone ultrasonic bath at room temperature for 10 min. HPFS wafers achieved better liftoff using the NMP bath, while Si wafers were more successful in acetone. Wafers were then cleaned with isopropyl alcohol (IPA) and deionized water, followed by a 3 min oxygen plasma descum. Ni liftoff on HPFS wafers resulted in nearly all the deposited metal being removed; however, Si wafers did not experience this issue. The Ni deposition was therefore repeated on the HPFS wafers, using 10 nm of Ti as a seed layer to improve adhesion. The Au deposition also used a 10 nm Ti base layer on all wafers for similar reasons.

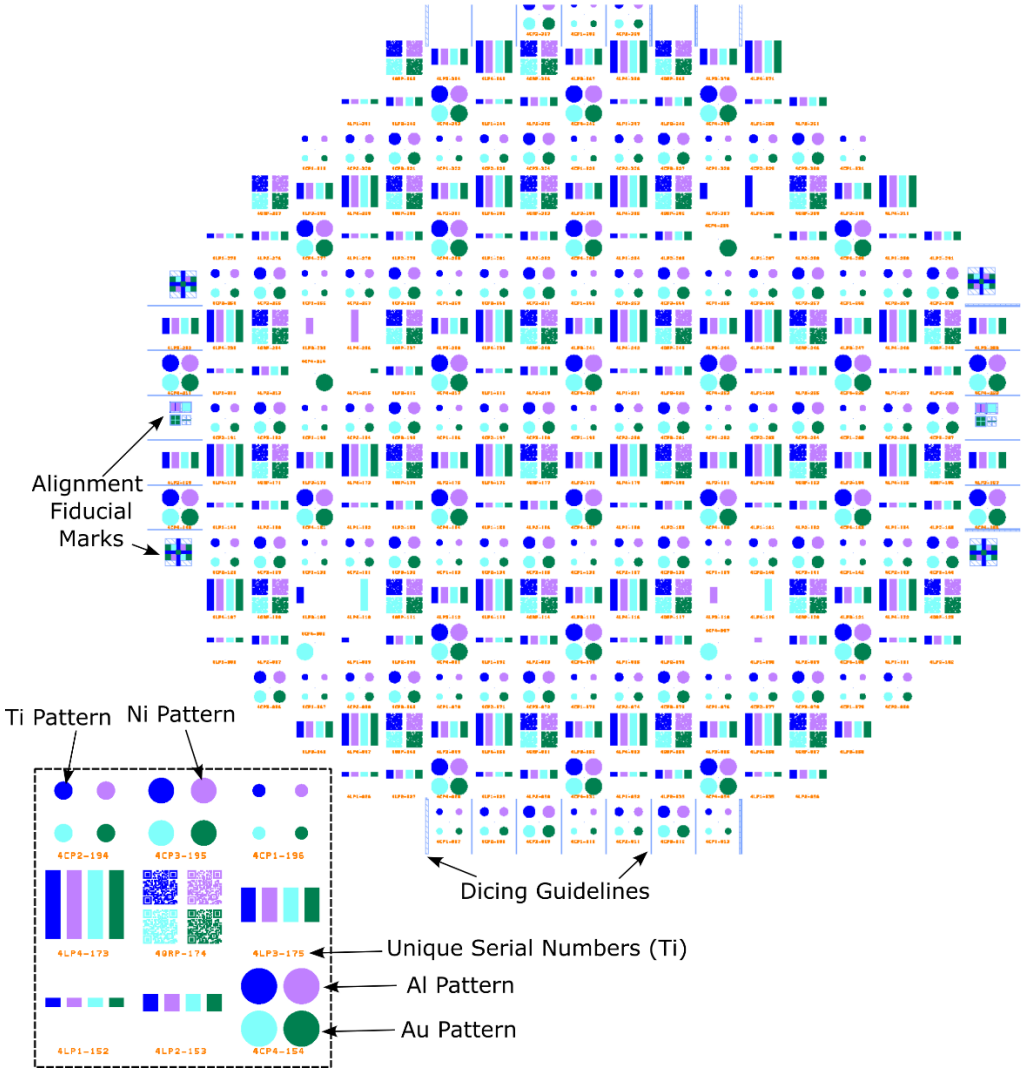

Figure 1. Overlay of the five photomasks used to fabricate MFM devices on 100 mm diameter wafer. Each color corresponds to a separate photomask pattern.

Table 2. Metal deposition thicknesses for coplanar MFM devices

Deposition Step	Material	Nominal Thickness (nm)	Purpose	Notes
1	Ti	200	Dosimeter material	
2	Al	200	Dosimeter material	
3	Ti/Ni	10/200	Dosimeter material	Si wafers did not have a Ti adhesion layer
4	Ti/Au	10/20	Dosimeter material	
5	Ti	50	Device serial number	

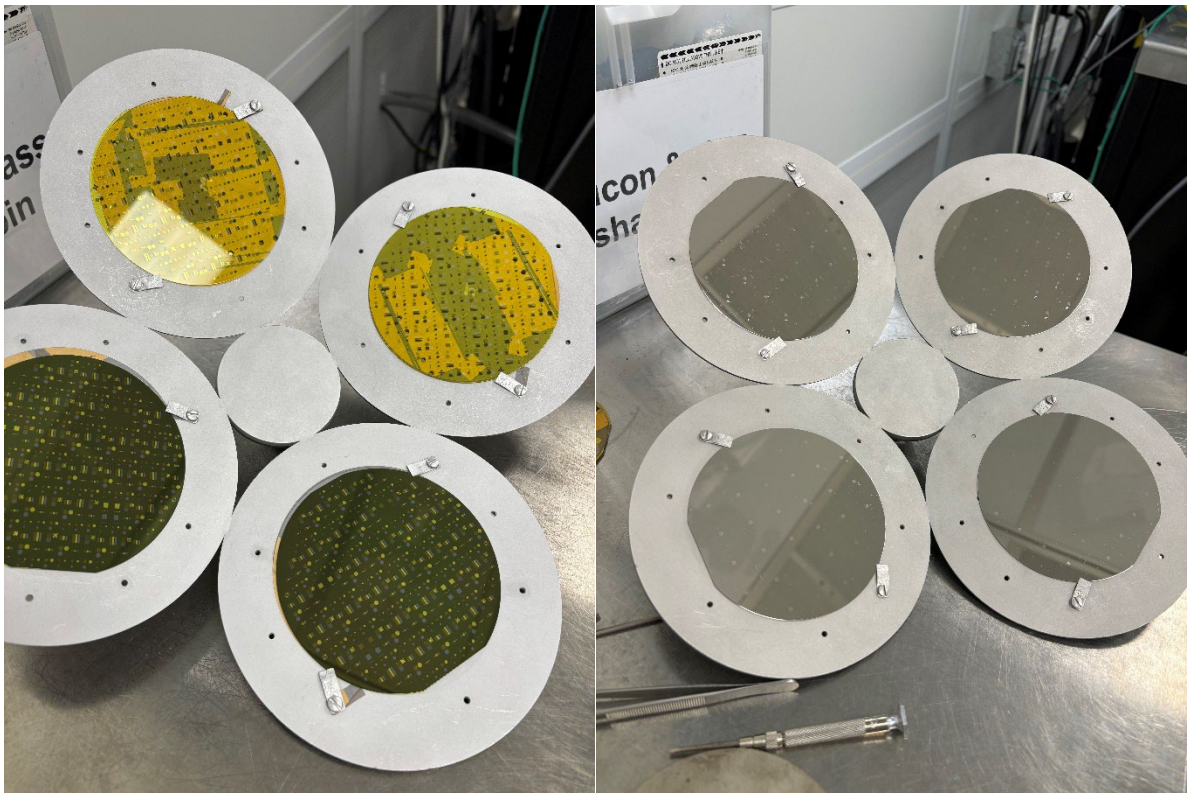

Figure 2. Wafers secured to e-beam orbital plate before (left) and after (right) titanium deposition.

Colinear (stacked) MFM devices used a slightly different photolithography process than the coplanar devices because of the thicker metal deposition. AZ-5214E-IR resist (Clariant Corporation, Somerville, NJ) was spin coated onto wafers at 2,000 rpm for 45 s for a nominal resist thickness of 1.98 µm. Wafers were patterned using the Suss MA6 aligner and developed using AZ 300 series developer. Then, 200 nm layers of Ti, Al, and Ni, along with 20 nm of Au, were evaporated in a single e-beam deposition process, followed by liftoff in acetone. A second Ti deposition was also performed on colinear devices to pattern device serial numbers. However, the Ti did not adhere to the Si, likely because of residual photoresist from the initial deposition. To avoid this issue with other wafers, the oxygen plasma descum process was added following liftoff.

The 300 µm Si wafer received a 20 nm Al_2O_3 conformal coating using a Lesker atomic layer deposition tool. This coating was intended to serve as a protective film to avoid scratching or oxidizing the deposited metals during irradiation and high-temperature testing. Wafers were then spin coated with Microposit SPR 955CM-0.7 photoresist (Dow Chemical, Midland, MI) before wafer dicing. The wafers were cut into a 5 × 5 mm die size using an Accretech automated dicing saw. Individual devices were then cleaned in acetone and IPA and sorted according to device size and layout. Approximately 1,250 MFM devices in total were produced from 5 wafers. One set of coplanar MFM devices produced from a HPFS wafer is shown next to a dime for scale in Figure 3. Looking at one of the rectangular MFM devices (top row), the metals are ordered Ti, Al, Ni, and Au from left to right. Serial numbers at the bottom of each device are readable by eye or with slight magnification, and QR codes are readable using a smart phone camera. The text of the QR reads: “MicroFluxMonitorProtoV0.”

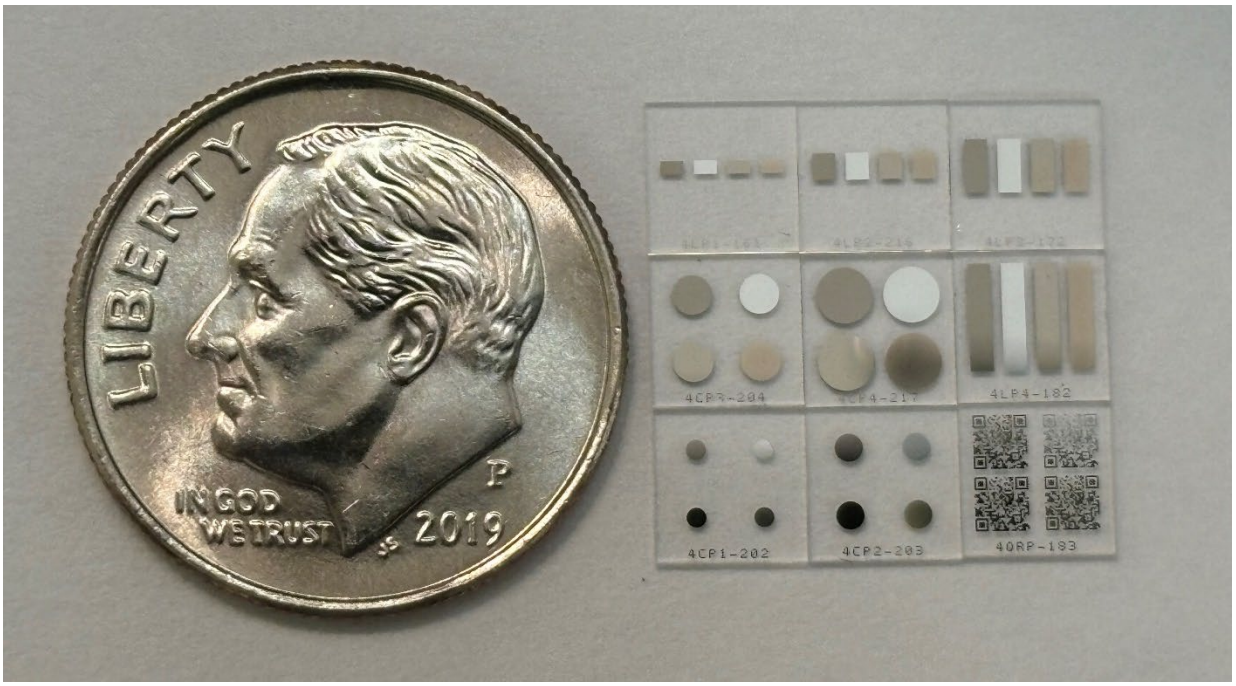

Figure 3. MFM coplanar devices of each size on HPFS substrates.

2.1 PRE-IRRADIATION CHARACTERIZATION

While the deposition rate of each metal was monitored using a crystal monitor in the e-beam tool, a KLA-Tencor P-6 stylus profilometer was used to measure the metal contact height on select devices. The profile of each metal in five locations on the 500 µm Si wafer was measured, with locations indicated in Figure 4. The average contact height measured in each location is listed in Table 3. For Ti, Al, and Ni, the values represent the actual contact height. The thicknesses shown for Au were reduced by a nominal 10 nm to account for the Ti below the Au contact to help with adhesion.

Table 3. Device metal height (nm) on 500 µm Si wafer measured using profilometer

Figure ID	Device ID	Ti	Al	Ni	Au
1	4CP3-192	195	173	165	13
2	4LP3-178	201	178	169	19
3	4CP3-207	208	203	174	11
4	4LP3-367	187	179	160	19
5	4LP1-029	199	182	169	19
	Average	**198**	**183**	**167**	**16**
	std	**8**	**12**	**5**	**4**

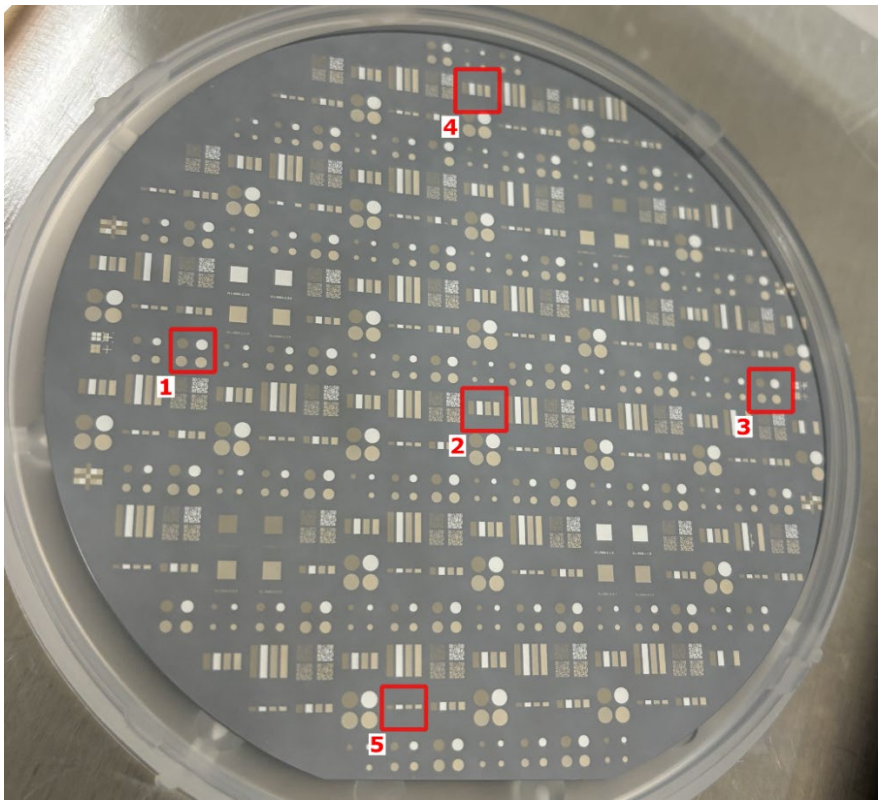

Figure 4. Device locations on wafer measured using profilometer.

MFM devices from the 300 µm wafer were individually weighed to determine variability between specimens. Three randomly selected devices of each size were massed, with the results illustrated in Figure 5. Average masses for devices from the 500 µm Si wafer and HPFS wafer were 29.5 ± 0.2 mg and 26.6 ± 0.3 mg, respectively.

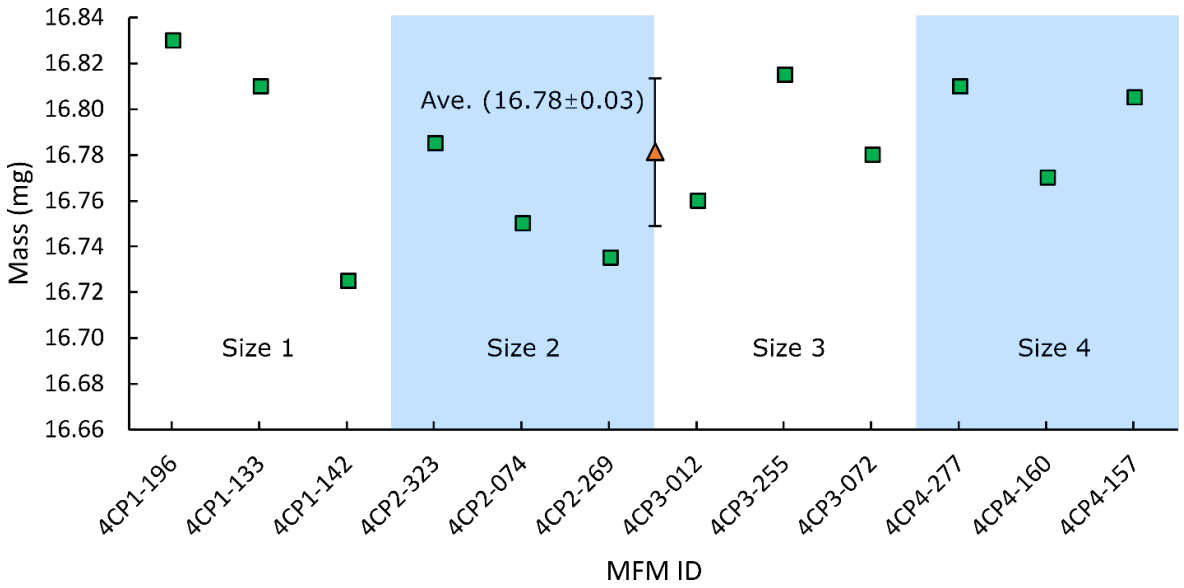

Figure 5. Mass of individual MFM devices on 300 µm Si (green squares) and average device mass (orange triangle).

Using the surface area of each metal contact calculated by the photomask design software and the average contact height measured with a profilometer, the volume and mass of each size device for each metal was calculated and summarized in Table 4. This assumed each material was deposited at full density.

Table 4. Surface area and total mass of MFM metal contacts

MFM Device	Surface Area (mm^2)	Metal Mass (µg)			
		Ti	Al	Ni	Au
Size - 4	2.625 ± 0.011	2.34 ± 0.10	1.30 ± 0.09	3.90 ± 0.12	0.81 ± 0.20
Size - 3	1.313 ± 0.008	1.17 ± 0.05	0.65 ± 0.04	1.95 ± 0.06	0.41 ± 0.10
Size - 2	0.656 ± 0.006	0.58 ± 0.02	0.32 ± 0.02	0.98 ± 0.03	0.20 ± 0.05
Size - 1	0.328 ± 0.004	0.29 ± 0.01	0.16 ± 0.01	0.49 ± 0.02	0.10 ± 0.03
QR code	1.555 ± 0.009	1.39 ± 0.06	0.77 ± 0.05	2.31 ± 0.07	0.48 ± 0.12
NAA sample	4.233 ± 0.015	3.77 ± 0.15	2.09 ± 0.14	6.29 ± 0.19	1.31 ± 0.33

3. MFM TESTING

3.1 REACTOR TESTING

MFM devices were irradiated in HFIR using the NAA Laboratory during HFIR cycles 507 and 508. Fourteen capsules were irradiated in high density polyethylene (HDPE) or graphite capsules for a total of 40 MFM devices and 5 sets of standard flux monitor foils. An overview of the irradiation campaign is shown in Table 5. Standard flux monitor foils were irradiated for 20 and 30 s in PT-1 and PT-2, respectively, on each day of irradiation to measure the facility neutron flux. The standard flux monitors are small, dilute disks of dispersed Au (0.10 wt%) in Al and Mn (0.0879 wt%) in Al. The activity in these disks was measured following irradiation and was used to determine the total and thermal flux in the facility using a one group collapsed cross section. The mass of each flux monitor foil and the dilute Au and Mn mass are shown in Table 6.

Table 5. Details of irradiation performed on MFM devices, including the end of bombardment (EOB) time, facility, and irradiation duration

HFIR Cycle	Irradiation Date	EOB	Facility	Duration (s)	Rabbit Capsule	Capsule Name
507	6/26/2024	12:25:09	PT-2	30	HDPE	FM-69
507	6/26/2024	12:28:07	PT-1	20	HDPE	FM-01
507	6/26/2024	13:07:40	PT-2	30	HDPE	Blank Si
507	6/26/2024	16:22:13	PT-1	60	HDPE	MFM Spots
507	6/28/2024	8:37:30	PT-1	60	HDPE	MFM Lines
507	6/28/2024	8:39:35	PT-1	60	HDPE	MFM QR
508	8/7/2024	11:26:08	PT-1	20	HDPE	FM-64
508	8/7/2024	12:29:02	PT-1	60	HDPE	Line-MFM
508	8/7/2024	13:09:36	PT-1	60	HDPE	2C2L MFM
508	8/7/2024	13:59:33	PT-1	60	HDPE	507 Line MFM
508	8/8/2024	7:46:49	PT-1	20	HDPE	FM-42
508	8/8/2024	13:55:07	PT-1	1800	Graphite	Graphite LU 111
508	8/14/2024	11:00:58	PT-1	20	HDPE	FM-27
508	8/14/2024	11:34:58	PT-1	60	HDPE	3CU

Table 6. Mass of dilute flux monitor foils used for comparison with MFM device

Flux Monitor	Dilute Au		Dilute Mn	
	Foil Mass (mg)	Au mass (µg)	Foil Mass (mg)	Mn mass (µg)
FM-69	67.9 ± 0.1	67.9 ± 0.1	20.9 ± 0.1	18.4 ± 0.1
FM-01	67.2 ± 0.1	67.2 ± 0.1	19.5 ± 0.1	17.1 ± 0.1
FM-64	67.3 ± 0.1	67.3 ± 0.1	20.9 ± 0.1	18.4 ± 0.1
FM-42	70.10 ± 0.01	70.10 ± 0.01	21.46 ± 0.01	18.86 ± 0.01
FM-27	70.60 ± 0.01	70.60 ± 0.01	21.65 ± 0.01	19.03 ± 0.01

Individual MFM devices were enclosed in HDPE subcapsules and stacked inside of HDPE rabbits, as shown in Figure 6. This separation of devices was performed to mitigate potential scratching or cross contamination of dosimeter metals during irradiation. The position of each MFM device in the rabbit was recorded to investigate neutron flux gradients along the length of the capsule, with position 1 corresponding to the topmost position during irradiation in HFIR. Rabbits that contained differently sized MFM devices were stacked in order of decreasing mass, with the smallest MFM devices on top. This allowed the samples with the lowest radioactivity to be retrieved first and undergo gamma spectrometry before the reaction products of interest decayed below the limit of detection. MFM devices in the graphite rabbit were wrapped in high-purity Al foil to mitigate contamination from the graphite rabbit itself. Samples in the graphite rabbit were NAA samples and contained only one of the dosimeter materials on each device (Al, Ti, Ni, or Au) to investigate impurities in the deposited metals. Two NAA samples of each material from the undoped Si wafer were colocated in each Al foil packet. The Al_2O_3 coating on these samples helped to avoid scratching or cross contamination between devices.

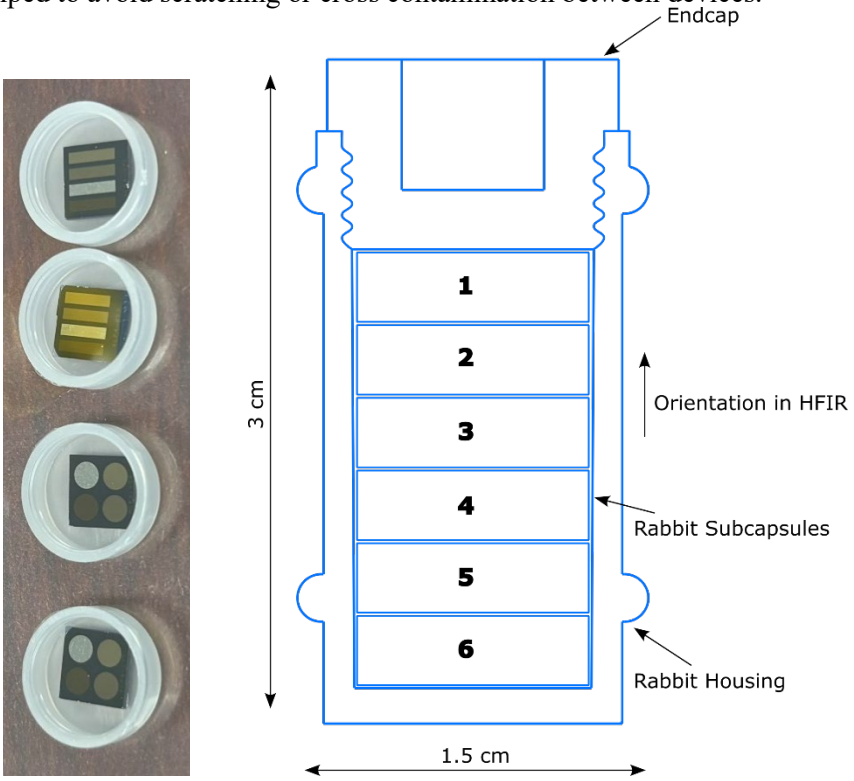

Figure 6. Devices loaded into subcapsules for 2C2L MFM rabbit capsule (left) and schematic of HDPE rabbits used in HFIR testing (right) with numbers corresponding to subcapsule positions.

Assembled rabbits were then sealed by rotating a soldering iron circumferentially around the interface between the endcap and rabbit housing. This prevents the possibility of the endcap unseating and becoming stuck in the PT during irradiation. Irradiation testing began by irradiating blank Si wafers in the PT-2 location, which has a lower thermal neutron flux ($\sim 4 \times 10^{13}$ n/cm^2/s) relative to the PT-1 location ($\sim 4 \times 10^{14}$ n/cm^2/s). This served as a precautionary irradiation to look for signs of thermal damage (melting or darkening of the HDPE housing) and to perform NAA on the blank wafer to investigate impurities in the substrate material. Preliminary tests in PT-2 did not indicate signs of damage to the sample or rabbit, and all subsequent testing was performed in PT-1. The majority of MFM device testing used 60 s irradiation intervals, while one test with a graphite rabbit lasted for 30 min. The 30 min irradiation was performed to accumulate higher neutron fluence on the samples and produce detectable quantities of radionuclides with small cross sections, such as the threshold reactions in Ni and Ti.

Following irradiation, rabbits were disassembled and subcapsules were placed into labeled plastic vials for gamma spectrometry. All samples surveyed sufficiently low radioactivity (<100 mR/h), which allowed handling of the plastic vials. MFM devices were placed metal contact side down on top of a 10 cm tall hollow stand inside of a Pb shielded cavity. Spectra were acquired using an energy-calibrated Canberra coaxial HPGe detector connected to a Lynx multichannel analyzer. The majority of counting times were 300 s, with several longer counts on NAA samples irradiated in graphite rabbits. Acquired spectra were then processed using the Genie 2K spectroscopy software suite to identify photopeaks in the spectra. The software attempts to match photopeak centroids to the decay gamma energies of several hundred radioactive isotopes in a reference library. If successfully identified, the software uses the half-life of the identified isotope, the detection efficiency of the HPGe system, and the time between counting and irradiation to determine the activity of the isotope at the end of irradiation. This decay and efficiency correction was particularly important for this experiment since the majority of samples were measured sequentially on the same HPGe system. Without this correction, the radioactivity of similar MFM devices irradiated under similar conditions could appear drastically different because of different lengths of time between irradiation and spectrometry.

3.2 HIGH-TEMPERATURE TESTING

High-temperature testing of MFM devices was performed at 500°C for 64 h under a N_2 atmosphere. One sample of each geometry (circular, linear, QR code), from each substrate (N-type Si, undoped Si, and HPFS), along with a blank substrate material, was placed in a graphite crucible and loaded into a horizontal tube furnace. Pictures of the devices and individual masses were recorded before and after high-temperature testing to assess physical deformation or mass changes in the devices.

4. RESULTS

4.1 SUBSTRATE ANALYSIS

Blank substrates of each MFM material were irradiated and analyzed using gamma spectrometry to determine impurities in the substrate material, which could potentially interfere with measurements of activation products in the MFM metals. Gamma spectra from each sample, normalized to counting time, are shown in Figure 7, and nuclide activities identified by the Genie 2K software are shown in Table 7.

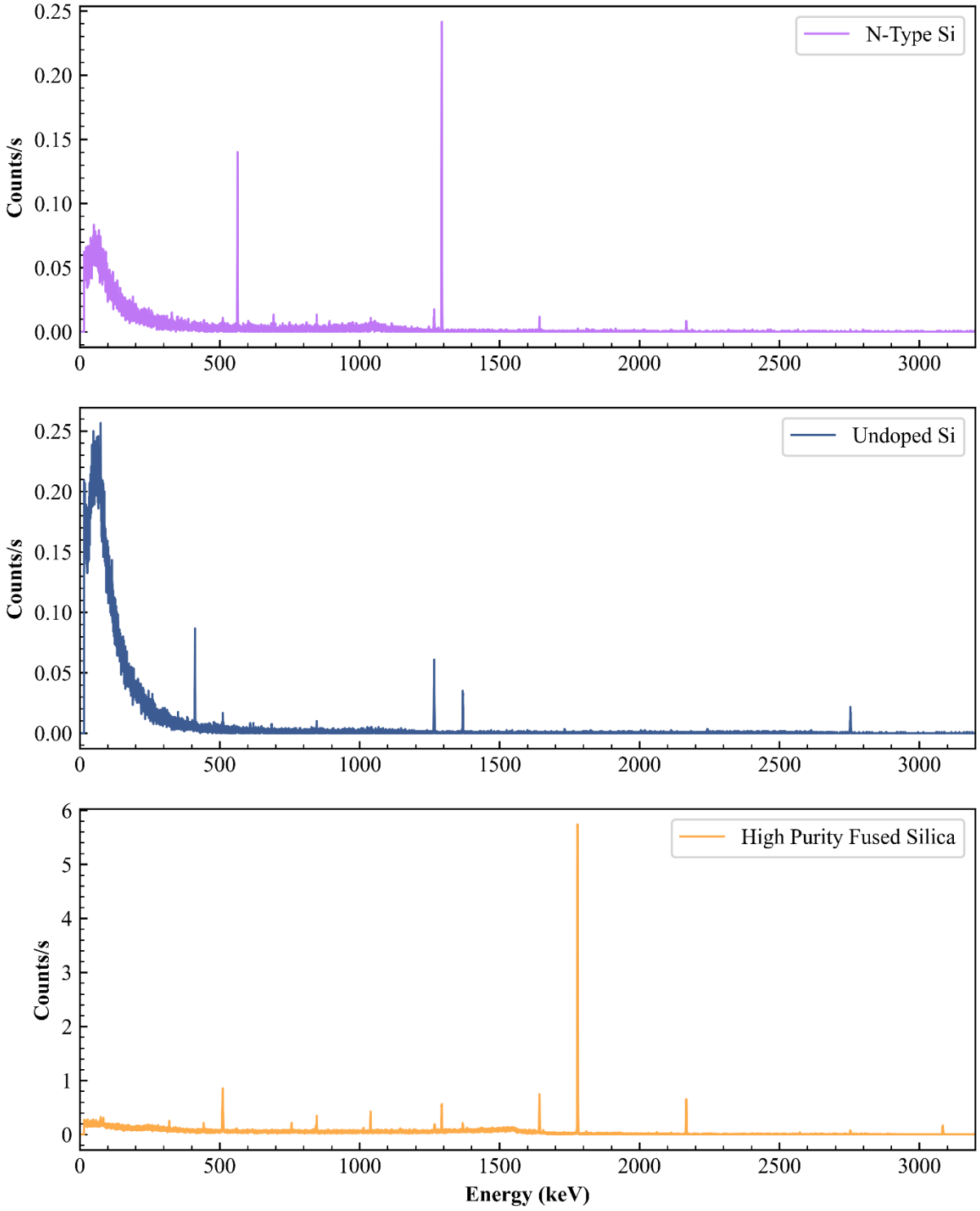

Figure 7. Gamma spectra, normalized to counting time, from blank N-type Si (top), undoped Si (middle), and HPFS (bottom) wafers.

Table 7. Identified nuclide activities in three blank wafers used for MFM substrates

Nuclide	Energy (keV)	HPFS		N-type SiC		Undoped Si	
		Activity (Bq)	Uncertainty	Activity (Bq)	Uncertainty	Activity (Bq)	Uncertainty
^{51}Cr	320.1	1,030	394	—	—	—	—
^{198}Au	411.8	—	—	—	—	135	14
^{128}I	442.9	1,810	553	—	—	—	—
^{64}Cu	511.0	5,860	382	—	—	—	—
^{122}Sb	563.9	—	—	351	25.7	—	—
^{56}Mn	846.8	1,070	129	—	—	—	—
^{66}Cu	1,039.2	82,700	41,100	—	—	—	—
^{41}Ar	1,293.6	2,270	181	2,680	124	—	—
^{24}Na	1,368.6	617	128	—	—	385	38.2
^{38}Cl	1,642.7	15,700	1,860	1,540	442	—	—
^{28}Al	1,779.0	1,290,000	39,500	—	—	—	—
^{56}Mn	1,810.7	692	212	—	—	—	—
^{56}Mn	2,113.1	579	289	—	—	—	—
^{38}Cl	2,167.7	15,200	2,310	1,770	478	—	—
^{24}Na	2,754.1	549	86.6	—	—	360	48.3
^{49}Ca	3,084.4	4,930	440	—	—	—	—

4.1.1 High-Purity Fused Silica

The 500 μm thick HPFS showed significantly high activity for a bare wafer with 777 total counts per second (cps), while the N-type Si and undoped Si had 56.8 and 142.6 cps, respectively. Most of this activity in the HPFS comes from ^{28}Al, which likely originates from the (n,p) reaction in ^{28}Si or neutron capture in ^{27}Al. However, the HPFS wafer was analyzed 9.4 min after the end of irradiation, while the N-Type and undoped Si samples were analyzed 2.3 and 18.5 h following irradiation, respectively. Aluminum-28 ($T_{1/2}$ = 2.245 m) and other short-lived isotopes in Table 7, such as ^{66}Cu, would have sufficient time to decay below the limits of detection in these two Si samples. Additionally, the HPFS sample inadvertently had a thin layer of photoresist, which could account for the other identified nuclides. Therefore, it is inconclusive whether the HPFS has a higher background contribution relative to the two Si wafers.

4.1.2 N-Type Si

The N-type Si showed a peak from ^{122}Sb at 563.9 keV, which was expected as Sb is used as an intentional N-type semiconductor dopant in this material. The other two dominant peaks observed in the N-type material were from ^{41}Ar and ^{38}Cl. Argon-41 is commonly observed in NAA measurements because of neutron activation of ^{40}Ar found in air. Air is the gas used to move rabbits into the reactor using the PT, and even though Ar constitutes less than 1% of air by volume, it transmutes to ^{41}Ar in significant quantities. Chlorine-38 likely comes from activation of trace Cl in the HDPE capsules.

4.1.3 Undoped Si

Undoped, 300 μm thick Si appeared to produce the lowest identifiable residual activity, with only ^{24}Na and ^{198}Au isotopes appearing in the spectrum. Sodium-24 is likely due to activation of ^{23}Na introduced by

salts or oil from contact with skin. Although samples were cleaned with acetone and IPA before assembling, residual salt on surfaces or tweezers could be the source. The ^{198}Au is likely due to trace quantities of Au adhering to the wafer during fabrication and should serve as a baseline for minimum Au background in these devices. Undoped Si samples were irradiated for 30 min, which is sufficient time to transmute very small quantities of Au. Argon-41 was not identified in the undoped Si, which might be because of the samples being wrapped in Al rather than being enclosed in plastic subcapsules. The plastic subcapsules could entrap air with ^{41}Ar, while the Al foil would allow ^{41}Ar to escape. The long delay between irradiation (18.5 h) is also sufficient time for ^{41}Ar ($T_{1/2}$ = 109 m) to decay below the limit of detection. Overall, although the undoped Si did produce a significant low-energy (<200 keV) continuum, the lack of the ^{122}Sb signature makes undoped Si a slightly better candidate than N-type Si for future device substrates.

4.2 HFIR TESTING

Multiple MFM devices were irradiated in HFIR during cycles 507 and 508 to investigate the relationship between metal contact size and activity, as well as the repeatability of activity for similar devices. Gold and its activation product ^{198}Au were the primary focus of this analysis, as the other reactions of interest in Al, Ni, and Ti were either too short lived to sequentially measure in all devices using one HPGe detector or did not receive enough neutron fluence to produce measurable quantities. All devices produced 0% detector deadtime at a 10 cm device to detector distance, even in devices analyzed several minutes after irradiation.

Figure 8 shows the gamma spectra, normalized to count time, after irradiating four different sizes of stacked MFM devices on N-type Si for 60 s. The 411.8 keV peak from ^{198}Au is clearly visible in each spectrum and increases in amplitude by a factor of two for increasing device size. The 563.9 keV peak from ^{122}Sb is also apparent in each spectrum and shows nearly the same count rate for each sized device. This is expected as the Sb is in the substrate material is present in the same quantity for each device. Higher energy, short half-life photo peaks, such as ^{198}Au (1,779 keV), are very clear in the smallest (size 1) device but become indiscernible for larger device sizes. This is not because of differences between samples but because of the order in which they were measured using the HPGe detector. As previously mentioned, the smallest sized samples were analyzed first to capture the lower activity ^{198}Au in the material. The time delay caused by sequential measuring results in the short-lived isotopes decaying below the limit of detection in some specimens. This is why the decay correction applied by the Genie 2K software was critical for comparing MFM devices as they were at the end of irradiation. This decay correction was very useful for some identified isotopes, such as ^{198}Au, but could not be used for radionuclides that decayed below the limit of detection. Figure 9 shows the same spectra in Figure 8 but on a semilog scale to show the gamma continuum caused by Compton scattering from high-energy gamma rays. This continuum reduces in intensity as the larger MFM devices are allowed to decay before counting.

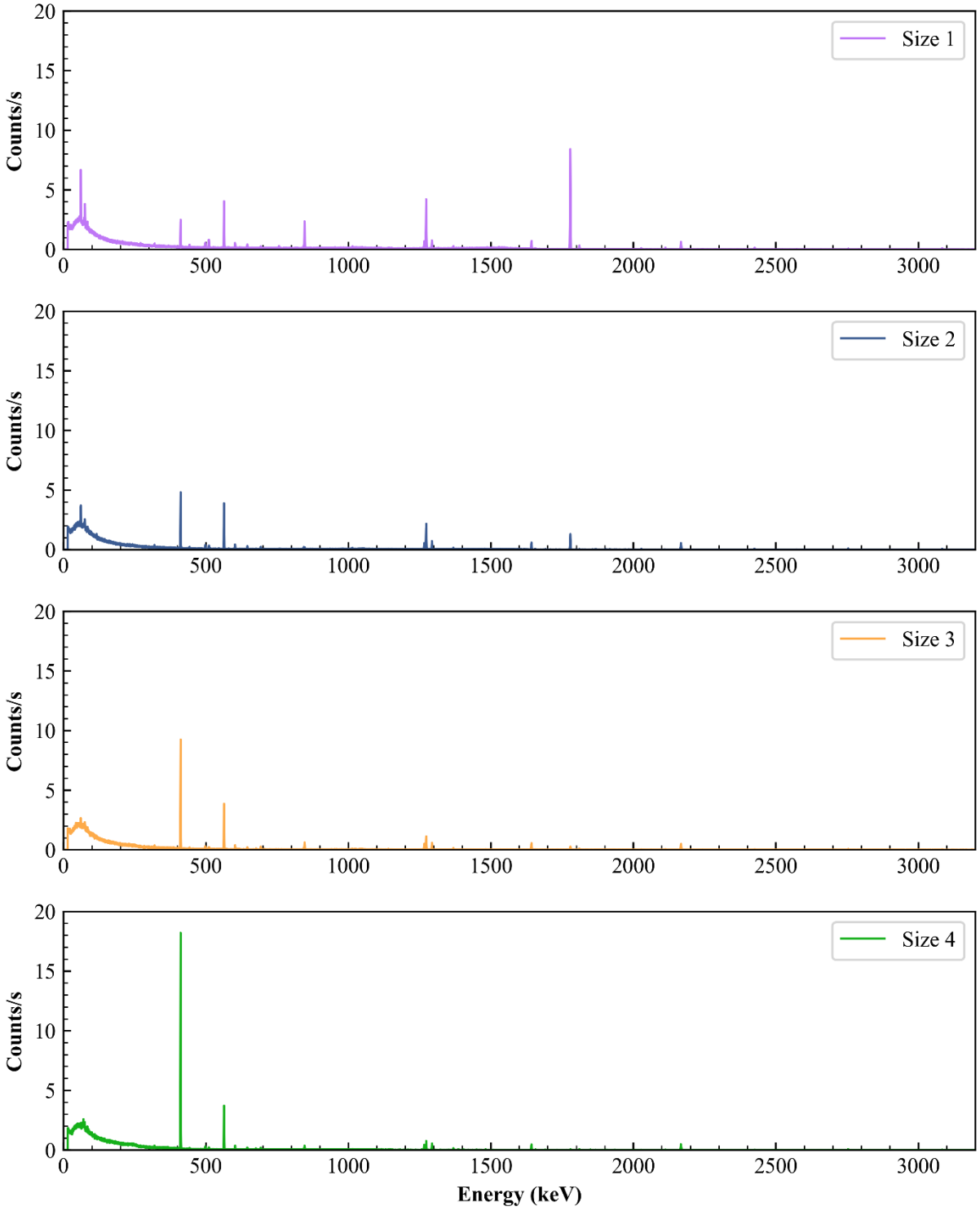

Figure 8. Normalized gamma spectra on linear scale from size 1–4 devices from *MFM Spots* capsule.

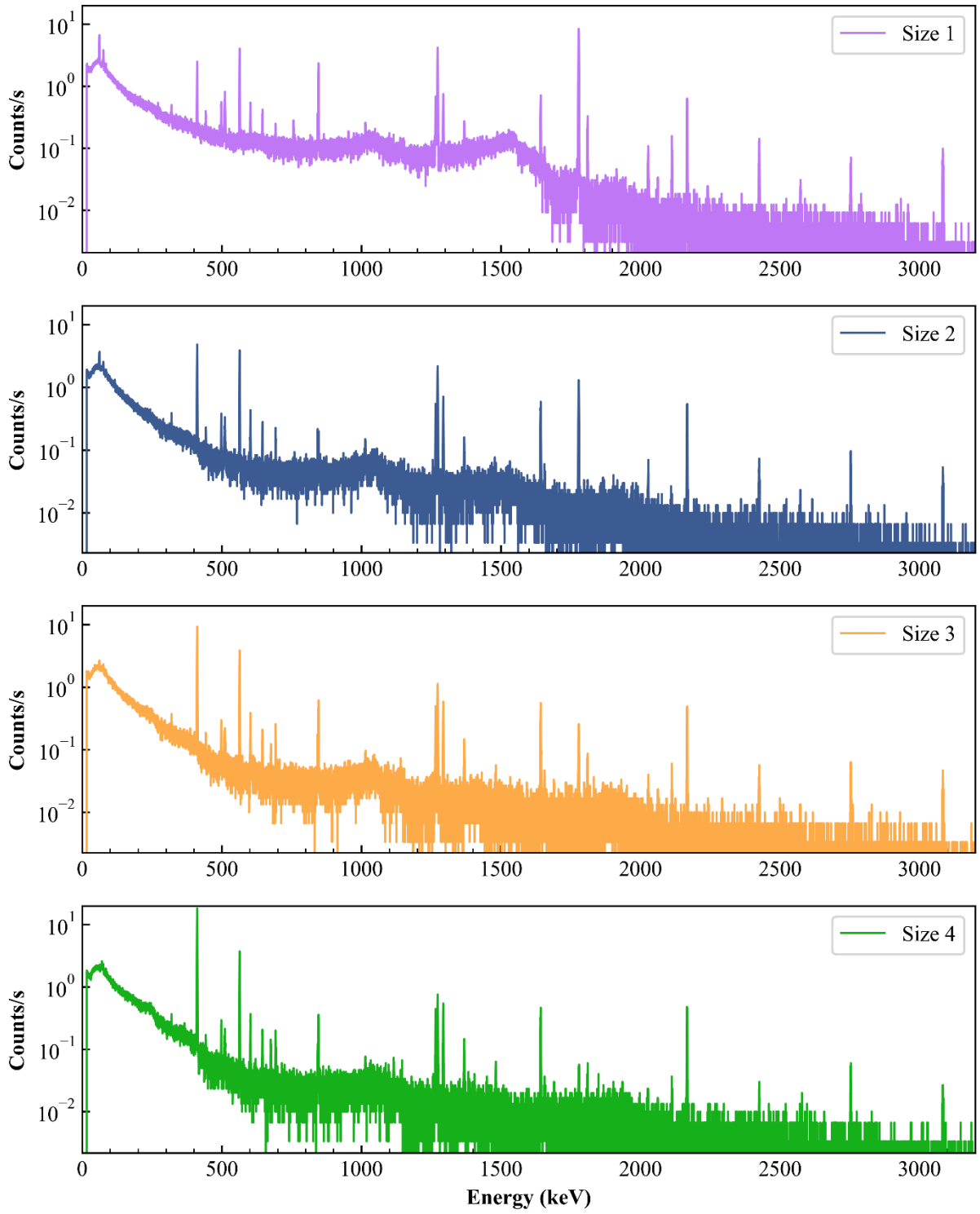

Figure 9. Normalized gamma spectra on semilog scale from size 1–4 devices from *MFM Spots* capsule.

To assess the linearity and reproducibility of MFM devices, the activity in ^{198}Au was the primary focus for statistical analysis. Figure 10 shows the ^{198}Au in four different sized MFM devices from three different irradiation experiments. Capsule *3CU* contained circular, coplanar geometries; capsule *Line-*

MFM contained linear, stacked geometries; and capsule *MFM Spots* contained circular, stacked geometries. As the figure shows, the ^{198}Au activity at the end of irradiation doubles in all capsules as the size of each device doubles. The uncertainty (2σ) associated with each activity also increases with increasing device size, which is somewhat unexpected. The number of photon counts in the 411.8 keV peak, before correcting for decay, doubles for each MFM device size which should reduce the relative uncertainty from 3.4% to 0.9%, since the relative error is proportional to the square root of the number of counts. However, the Genie 2K software calculates an uncertainty of approximately 5% for all sized devices. This discrepancy is likely because of other sources of uncertainty (detection efficiency, time, etc.) that propagate to a larger uncertainty in calculated activity.

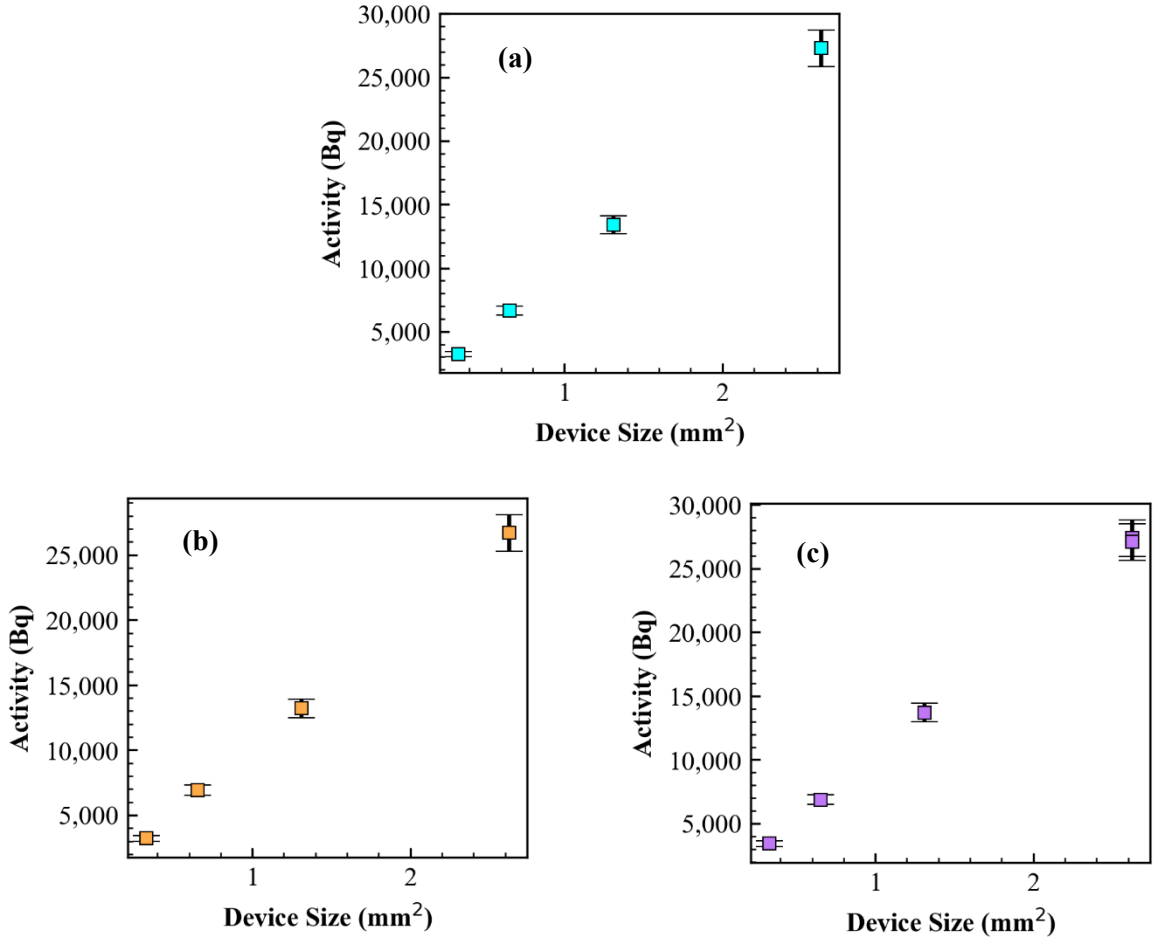

Figure 10. Total ^{198}Au activity in *3CU* (a), *Line-MFM* (b), and *MFM Spots* (c) irradiation capsules.One size of each device was included in each capsule.

For a better assessment of the linearity between differently sized MFM devices, the circular and linear devices were plotted together, as shown in Figure 11. A linear regression of these activities with respect to device size yielded an R-squared value of 1.000 at a 95% confidence interval, suggesting a highly linear relationship between MFM contact size and activity at the end of irradiation. When including all of the other devices irradiated for 60 s (Figure 12), the R-squared value decreases to 0.997 at a 95% confidence interval, again suggesting a highly linear relationship between device size and activity.

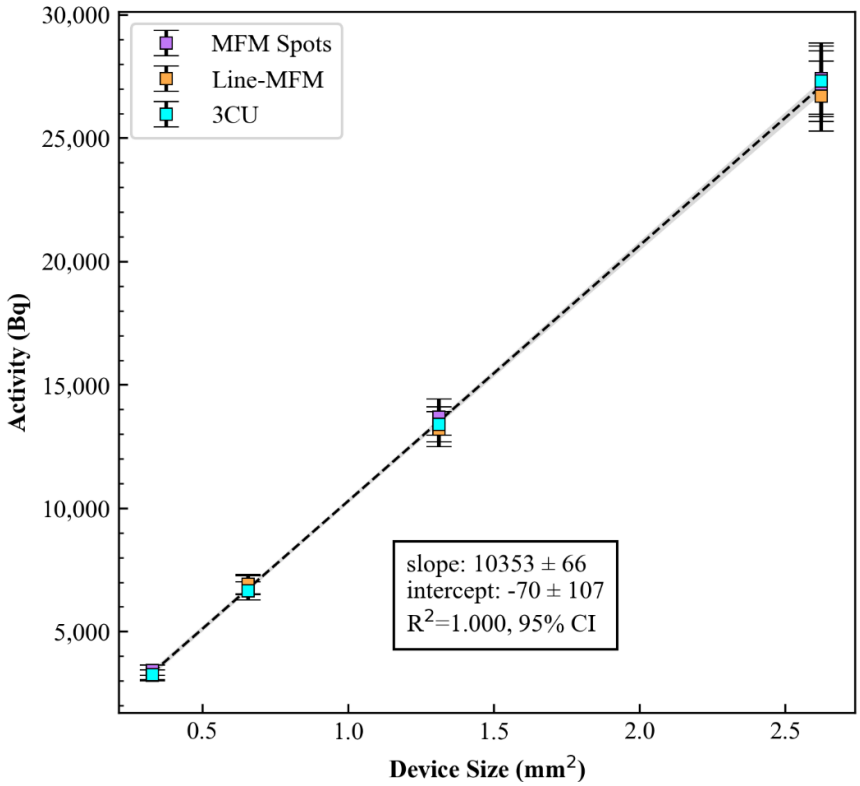

Figure 11. Linear regression of ^{198}Au activity in size 1–4 MFM devices with respect to Au contact area.

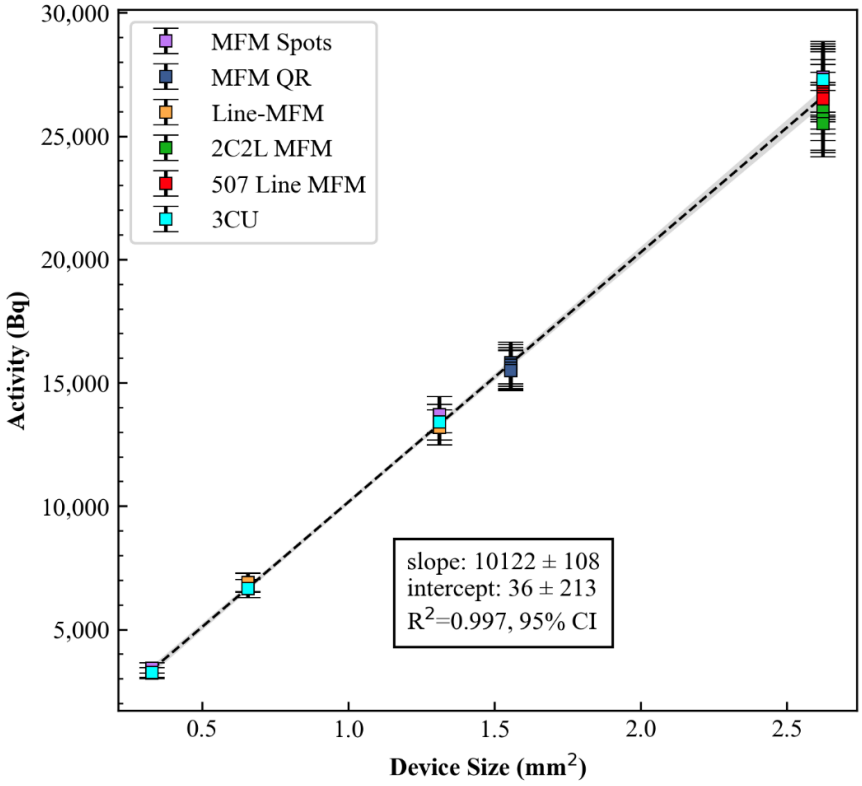

Figure 12. Linear regression of ^{198}Au activity in all MFM devices with respect to Au contact area.

Analyzing the activity of ^{198}Au in all of the size-4 MFM devices, Figure 13, shows similar activity between samples from different capsules. Specimens in the same capsule show even less variability in activity. Variations between capsules are evident but could be caused by the changing neutron flux over the course of a HFIR cycle. Figure 14 shows the measured ^{198}Au activity in dilute flux monitors irradiated at different points in the HFIR cycle. These also indicate subtle variations in activity from changes in neutron flux. The activity in these dilute monitors is also more than 27 times the activity of the size-4 MFM devices, despite being irradiated for one-third of the time.

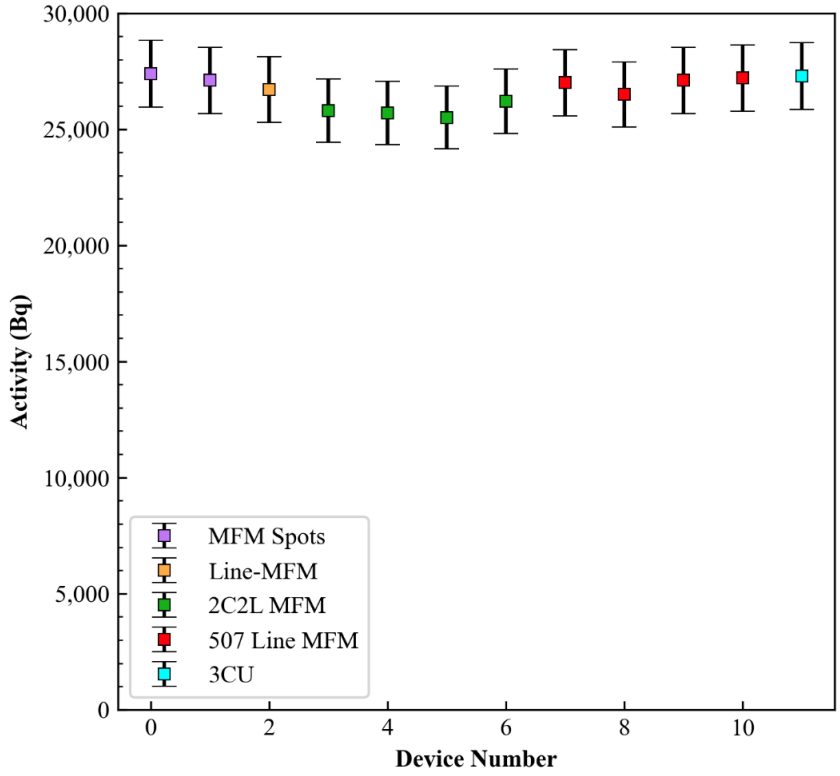

Figure 13. ^{198}Au activity in size-4 MFM devices.Device number is arbitrary.

To better asses the response of all sized MFM devices, the ^{198}Au activity was normalized to Au mass, as calculated in Table 4, and irradiation time. A plot of these normalized activities is shown in Figure 15, along with the average normalized activity between all devices (dashed line). As the figure indicates, the mean activity falls between the 2 σ uncertainty of all devices, suggesting very similar responses and reproducibility in all devices.

This activity normalization was extended to the dilute flux monitors to compare MFM devices and standard flux monitors irradiated on the same day. Figure 16 through Figure 19 show the normalized ^{198}Au activity for that day's flux monitor (white circle), each MFM device irradiated, and the average between MFM devices. Results show that the average MFM activity is very similar to the average activity of the flux monitor when normalized. In fact, all of the flux monitors appear to be equal to or less than the average MFM activity. This could be because of the negligible self-attenuation and self-shielding in the thin (16 nm) Au films on the MFM devices, resulting in slightly higher activity per unit mass.

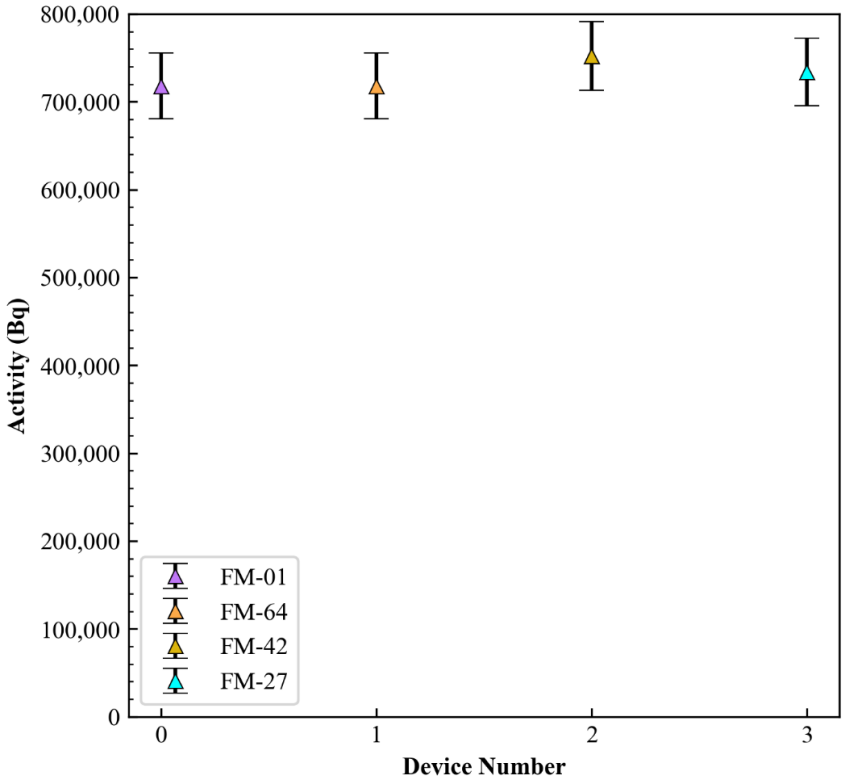

Figure 14. ^{198}Au activity in dilute Au/Al flux monitors. Device numbers are arbitrary.

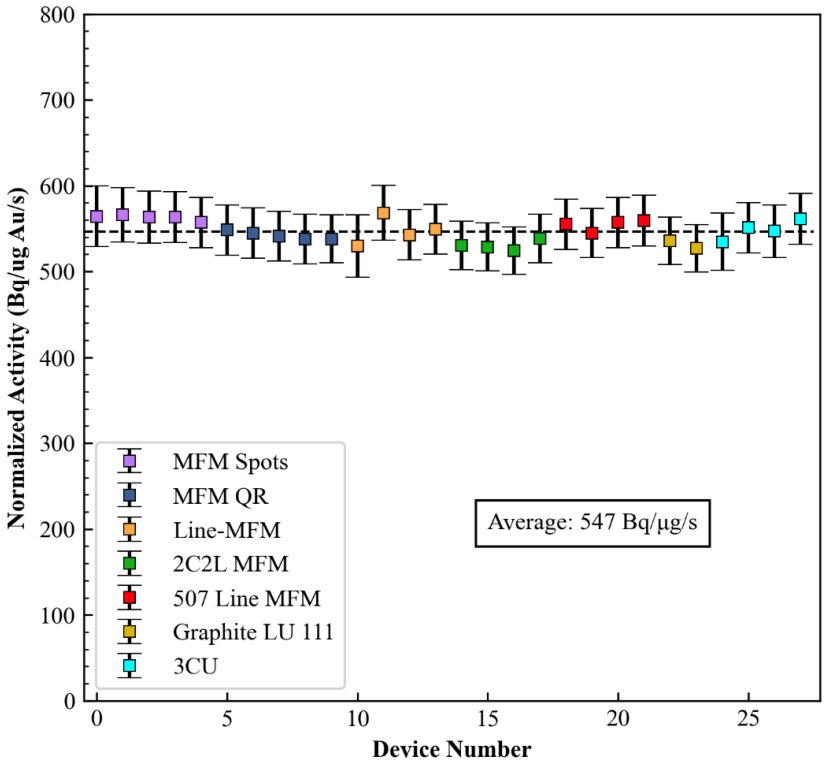

Figure 15. ^{198}Au activity normalized to Au mass and irradiation time for all MFM devices containing Au.

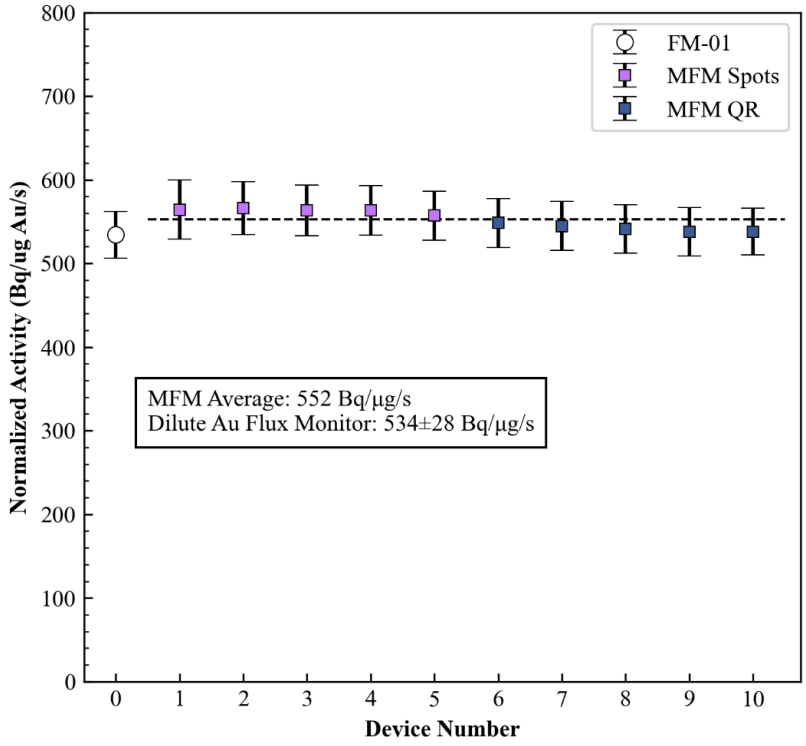

Figure 16. ^{198}Au activity normalized to Au mass and irradiation time for MFM Spots and MFM QR capsules, along with normalized ^{198}Au activity for dilute Au flux monitor FM-01 irradiated the same day.

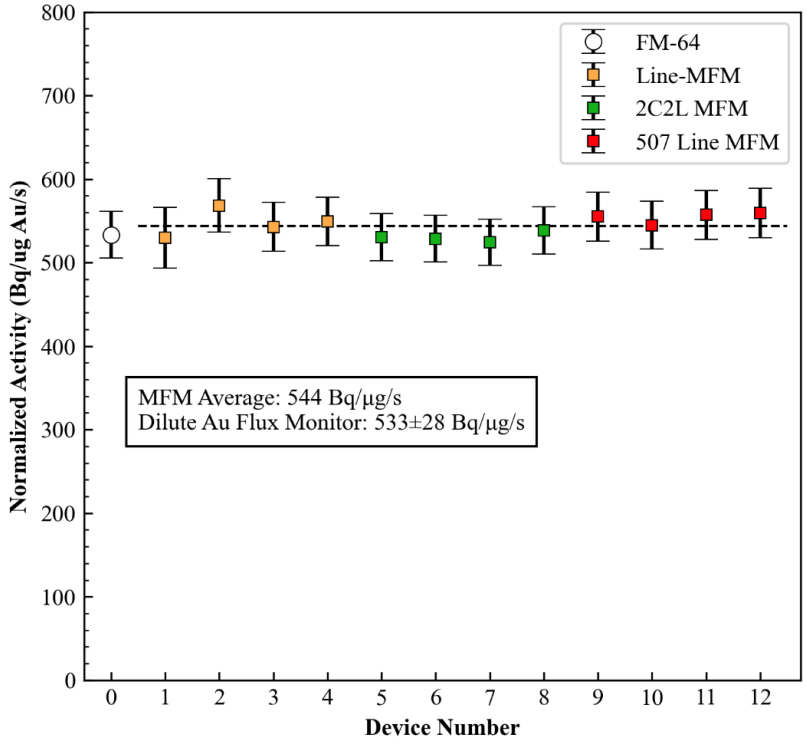

Figure 17. Normalized ^{198}Au activity for Line-MFM, 2C2L MFM, and 507 Line MFM capsules and for dilute Au flux monitor FM-64 irradiated the same day.

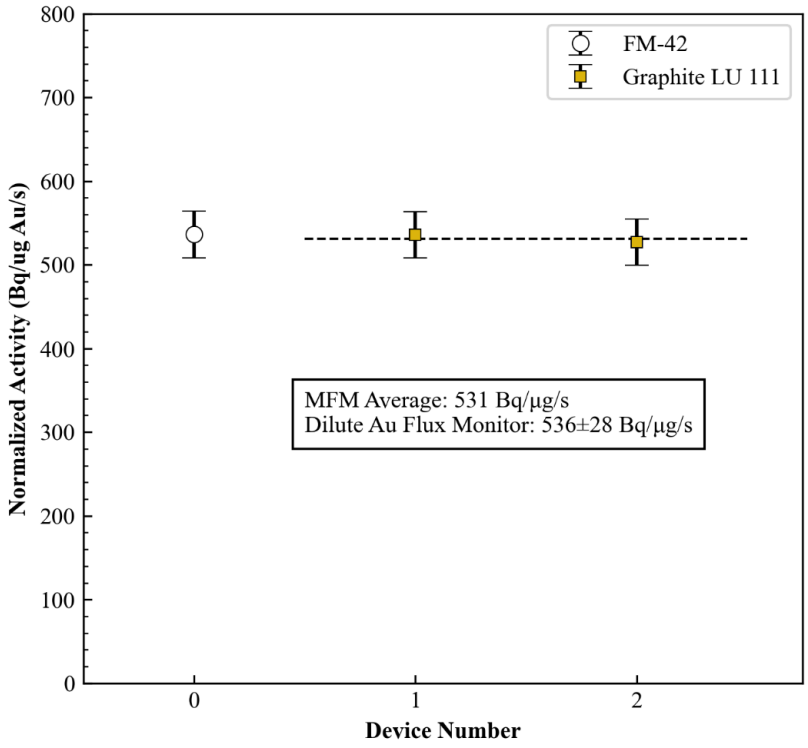

Figure 18. Normalized ^{198}Au activity for Graphite LU 111 capsule (irradiated for 30 min) and flux monitor FM-42 irradiated the same day.

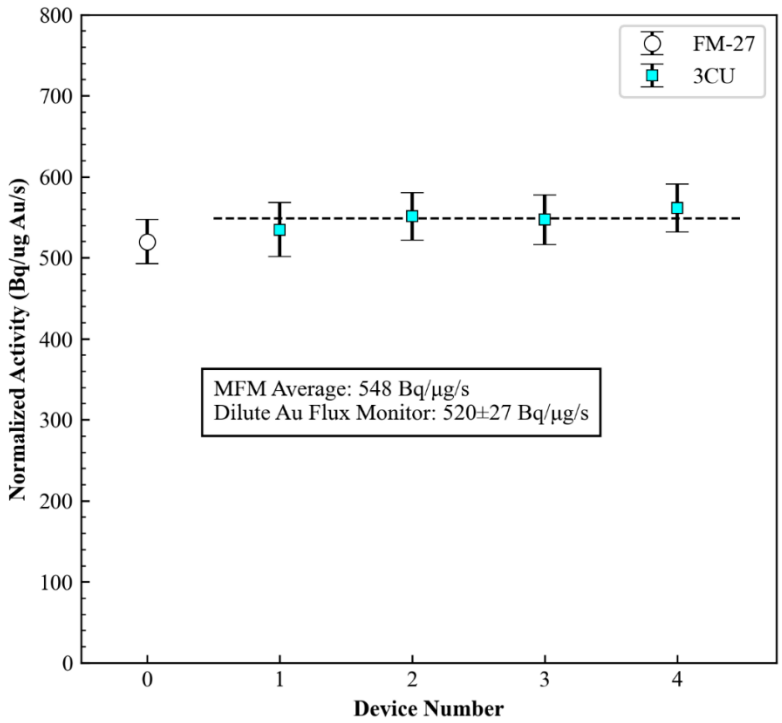

Figure 19. Normalized ^{198}Au activity for 3CU capsule and flux monitor FM-27 irradiated the same day.

Finally, the normalized activity for each MFM device in a given capsule was analyzed as a function of position. A linear regression through each normalized activity was performed, and the results are displayed in the insets of Figure 20. A statistical Wald test whose null hypothesis is that the slope = 0 was performed for each capsule. For all capsules except the *MFM QR* capsule, there was not sufficient evidence ($p < 0.01$) to reject the null hypothesis of zero slope. This means only capsule *MFM QR* indicated a detectable flux gradient over the capsule length. However, further testing should be conducted to verify this gradient.

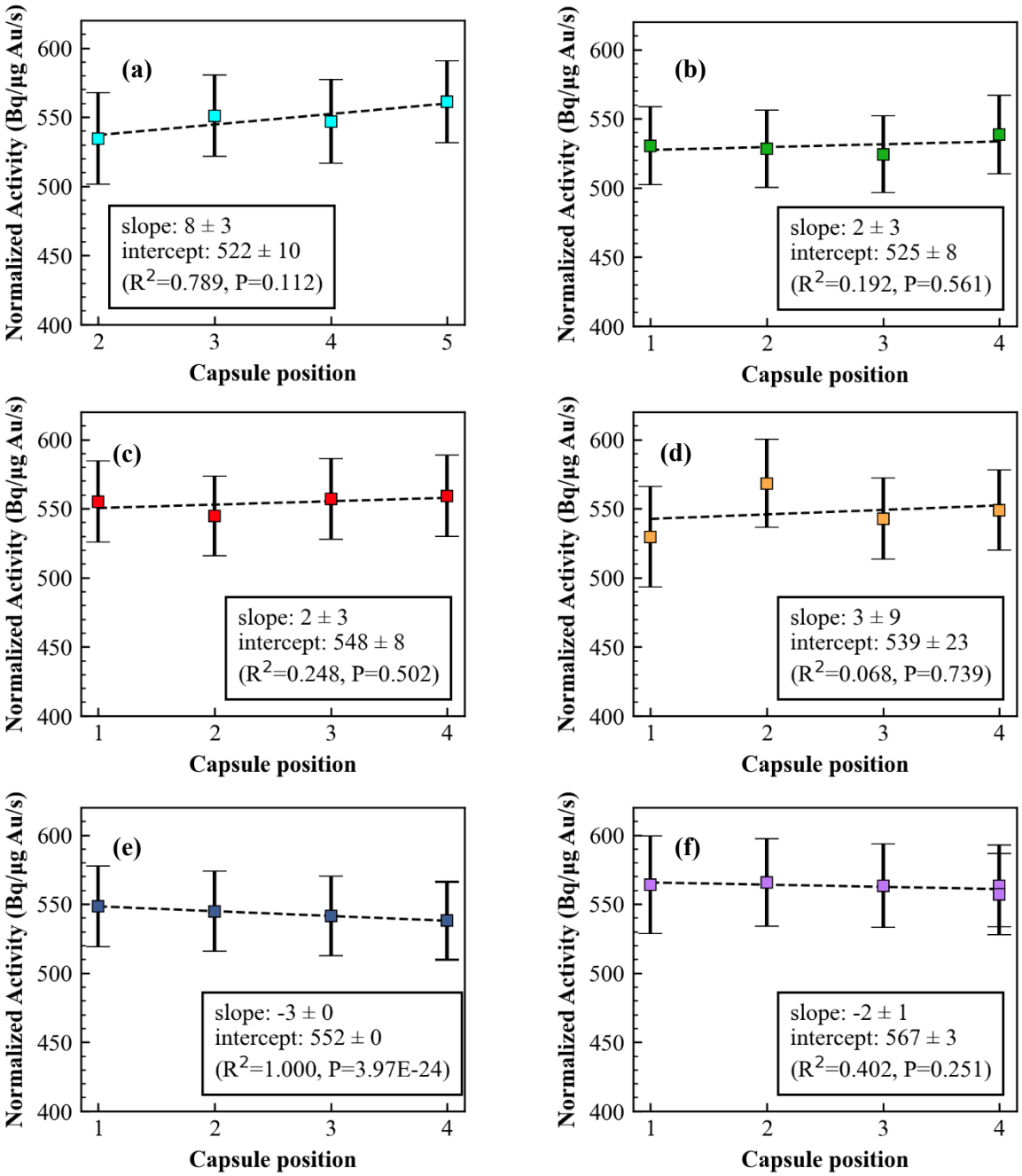

Figure 20. Normalized ^{198}Au activity in (a) 3CU, (b) 2C2L, (c) 507 Line MFM, (d) Line-MFM, (e) MFM QR, and (f) MFM Spots capsules, along with linear regression with respect to the device position in the capsule.

4.3 NAA SAMPLE ANALYSIS

NAA samples were irradiated in a graphite rabbit for 30 min in PT-1. Gamma spectra from each material are shown in Figure 21, and identified isotope activities at the end of irradiation are listed in Table 8. The majority of samples were gamma counted for 20 min, while the Ti sample was counted for 65 h, which is why significantly more isotope peaks were identified. The highlighted cells in Table 8 represent the activity of isotopes that were selected in a previous report [12] and were the intended nuclear reactions for these MFM devices. The activity of these isotopes, if produced in sufficient quantities, can be used for neutron spectrum adjustment calculations. However, ^{198}Au was the only isotope produced in significant quantities and used for determining neutron flux. This was expected since the neutron cross sections of the other reactions are very small and would require longer irradiations to produce significant quantities. Still, the fact that these isotopes were identified after a much shorter irradiation than the expected end use is very promising.

Table 8. NAA sample isotopic activity (Bq)

Isotope	Energy (keV)	NAA Sample			
		Ti	Ni	Au	Al
^{24}Na	1,368.6	213	172	191	278
^{24}Na	2,754.1	207	154	187	270
^{40}K	1,460.8	25.3	—	—	—
^{42}K	1,524.6	13.6	—	—	—
^{47}Sc	159.4	5.4	16.2	5,050	—
^{48}Sc	983.5	1.2	—	—	—
^{48}Sc	1,037.5	1.2	—	—	—
^{48}Sc	1,312.0	1.0	—	—	—
^{58}Co	810.8	—	12.3	—	—
^{60}Co	1,173.2	0.6	—	—	—
^{60}Co	1,332.5	1.1	—	—	—
^{64}Cu	511.0	271	534	—	913
^{65}Zn	1,115.5	—	22	—	—
^{115}Cd	336.2	0.9	—	—	—
^{115}Cd	527.9	1.1	—	—	—
^{122}Sb	563.9	0.4	—	—	—
^{187}W	479.6	70.3	958	—	—
^{187}W	618.3	80.7	984	—	—
^{187}W	685.7	73	989	—	—
^{188}Re	155.0	11.5	—	—	—
^{194}Ir	328.4	15.2	—	—	—
^{197}Hg	70.8	262	2,260	—	—
^{197}Hg	134.0	18.5	229	—	—
^{198}Au	411.8	421	6,200	1,240,000	1,530
^{241}Am	59.5	12.8	—	—	—

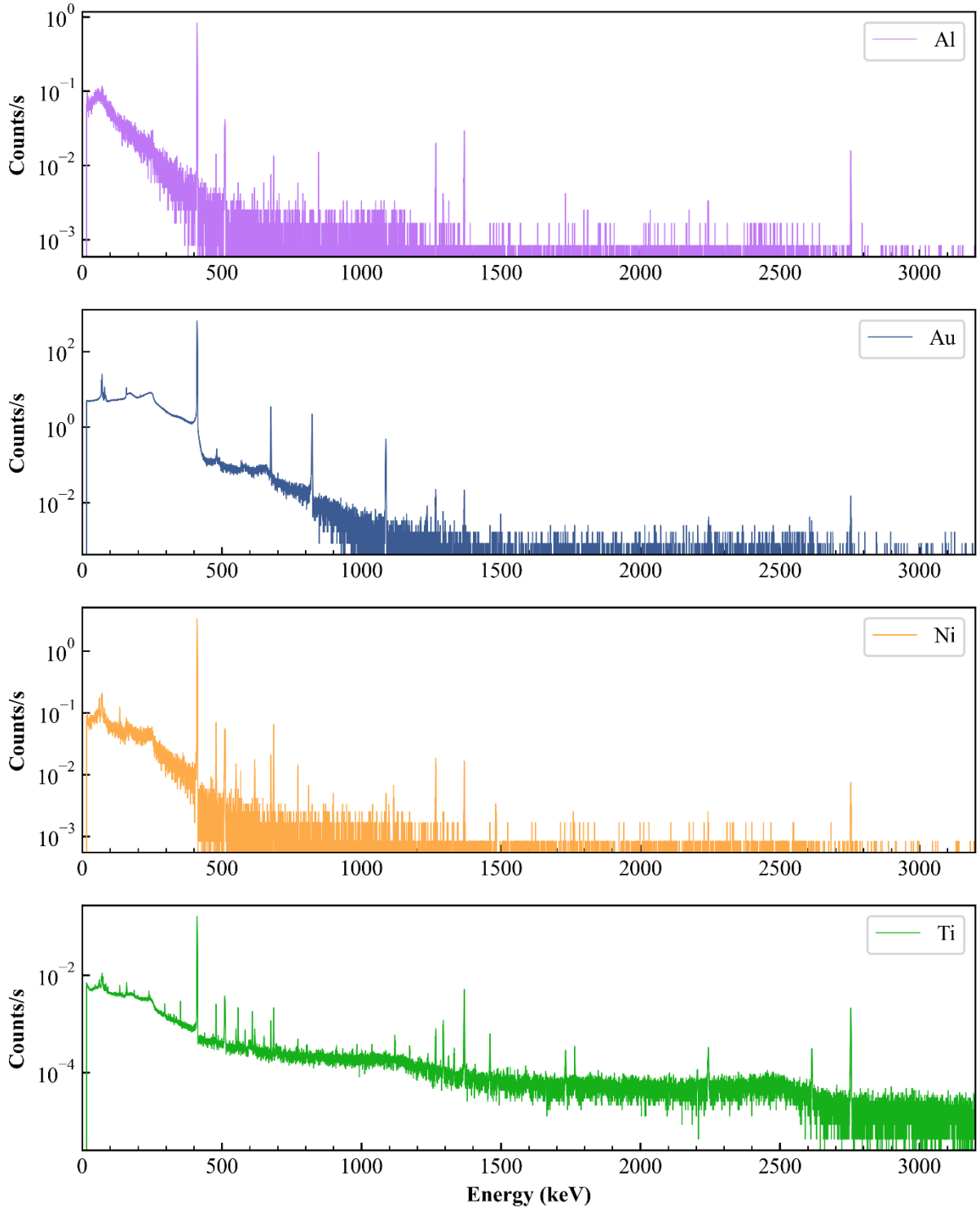

Figure 21. Gamma spectra from Al, Au, Ni, and Ti NAA samples.

4.4 NEUTRON FLUX MEASUREMENTS

^{198}Au activity in MFM devices was used to calculate total neutron flux in PT-1 using a one-group collapsed cross section for ^{197}Au capture. Total flux was also determined from measurements of the standard flux monitors, and the results are shown in Figure 22. As the figure shows, average MFM flux calculations (black dashed line) were within 3% of the standard monitor flux results (red solid line), indicating good agreement between the two.

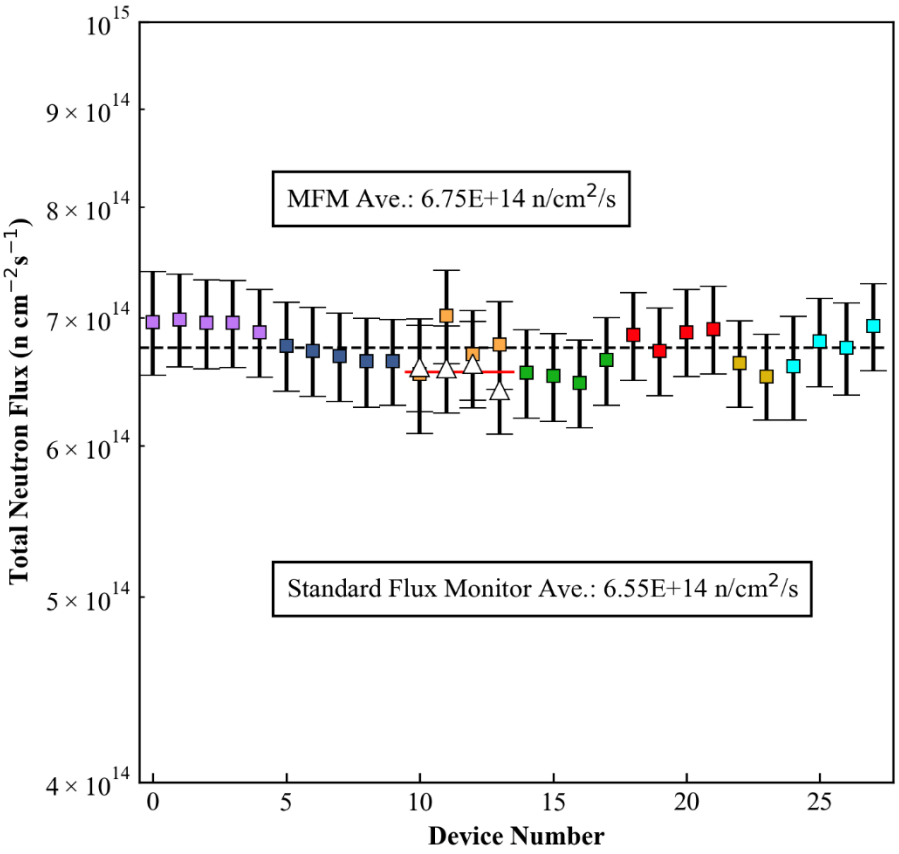

Figure 22. Total neutron flux measured using MFM devices (colored squares) and standard flux monitors (white triangles).The black dashed line represents the average total flux calculated for MFM devices, and the red solid line represents the average total flux calculated from flux monitors.

4.5 HIGH-TEMPERATURE TESTING

MFM devices were massed before and after high-temperature testing and showed negligible mass change. This is primarily evidence of the Si and HPFS stability in the N_2 environment, since the mass of the metals on the surface are below the measurement limit of the scale. With respect to geometry, all MFM devices performed well and did not appear to deform or reshape during heat testing. The QR codes on the devices were still readable with a cell phone camera, as were the alphanumeric serial numbers. Ti, Al, and Ni appeared to discolor on the uncoated coplanar devices (Figure 23). The Ti contacts appeared pale yellow, suggesting a TiN compound. Al also appeared yellow in color, which could indicate a thin film of AlN. The Ni contacts looked the most degraded with red and green patches on the surface, while the Au did not show any signs of changing.

The stacked MFM devices showed the most change from heat testing. The top stack metal was Au on these devices and appeared dark gray following testing. The Ti/Al/Ni/Au stack likely diffused while in the furnace, creating an alloy of all four metals. This is not necessarily an issue since the same quantity of each metal should remain in the stack. However, this has not been confirmed. Irradiation testing of the heat-treated devices is planned for future experiments and should indicate whether diffusion is problematic.

The Al_2O_3-coated wafers appeared to be the least affected by high temperatures. The color of each metal contact appeared slightly altered, particularly Al which changed from a shiny gray to yellow or blue depending on the angle of incidence. This could be caused by densification of the coating, which appears uniform over the wafer. Overall, the coating performed well in protecting the underlying dosimeter metal and will be used in future devices.

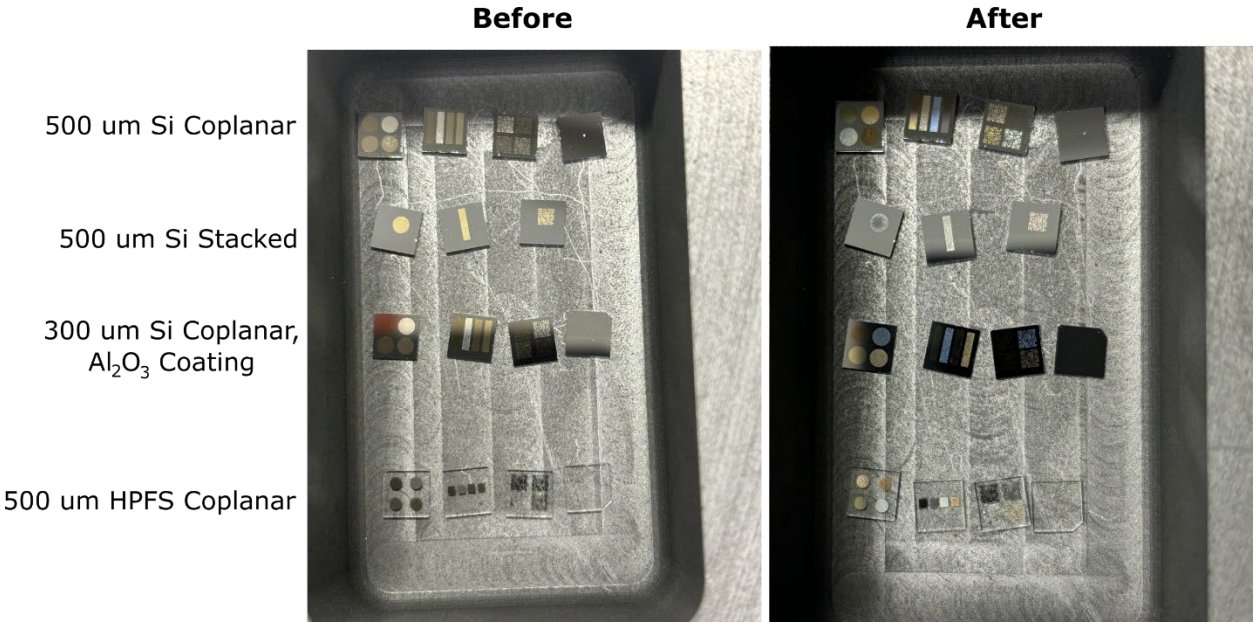

Figure 23. MFM devices of each substrate and geometry in a graphite crucible before and after 500°C testing.

5. CONCLUSIONS

Neutron dosimetry is a critical technique to measure the neutron flux, fluence, and energy spectrum of nuclear reactors and can be used to indicate fuel reloading, high-power operations, or changes in cycle length, which are of interest for safeguards monitoring. This work presents results of a novel device named the *micro flux monitor*, which is a miniaturized neutron dosimeter made from Ti, Al, Ni, and Au metals deposited on Si and HPFS substrates using standard semiconductor fabrication techniques. Approximately 1,250 devices were made, and 40 were tested in the NAA Laboratory at HFIR. Findings of this work are summarized below.

- Au is an excellent fluence monitor material and makes for repeatable and linearly scalable micro-dosimeters.
- Undoped Si is the best candidate substrate material, particularly if it is thinner; however, N-type Si is also a suitable candidate. The efficacy of HPFS is still undetermined.
- A comparison of stacked versus coplanar MFM structure could not be completed because Au was the top layer in all devices. However, coplanar devices showed better results in high-temperature testing because each metal was physically separate from one another.
- Ti might not be a suitable dosimeter material since it is required as a seed layer for proper adhesion of other materials (Au and Ni).
- Clear substrates can complicate the fabrication process as the correct surface of the wafer can be easily confused.
- Impurities in each source metal (Ti, Al, Ni, and Au) material are quite low. However, trace amounts of metals such as Au can remain inadvertently on devices during the fabrication process. This can be mitigated through changes to the fabrication process in the future.
- Neutron flux measurements with MFM devices were within 3% of standard flux monitors, demonstrating the efficacy of these devices.
- MFM devices were measured using gamma spectrometry minutes after irradiation and produced 0% detector deadtime at 10 cm.
- MFM devices can withstand high-temperature environments (500°C) and could be deployed in high-temperature advanced reactors.

6. ACKNOWLEDGMENTS

This work was performed on behalf of the Advanced Reactor International Safeguards Engagement (ARISE) program in the US Department of Energy (DOE), National Nuclear Security Administration's Office of International Nuclear Safeguards. The authors appreciate the assistance of Dayrl Briggs, Bernadeta Srijanto, Sujoy Ghosh, Kevin Lester, and Dale Hensley in fabricating MFM devices, as well as Fue Xiong in performing high-temperature testing. MFM device fabrication was supported by the Center for Nanophase Materials Sciences, which is a DOE, Office of Science User Facility, at Oak Ridge National Laboratory.

7. REFERENCES

1. *Neutron Fluence Measurements*. Technical Reports Series No. 107, ed. International Atomic Energy Agency. 1970, Vienna: International Atomic Energy Agency,.
2. ASTM International, *ASTM E844 - Standard Guide for Sensor Set Design and Irradiation for Reactor Surveillance*, West Conshohocken, PA (2018).
3. ASTM International, *ASTM E264 - Standard Test Method for Measuring Fast-Neutron Reaction Rates by Radioactivation of Nickel*, West Conshohocken, PA (2019).
4. ASTM International, *ASTM E266 - Standard Test Method for Measuring Fast-Neutron Reaction Rates by Radioactivation of Aluminum*, West Conshohocken, PA (2017).
5. ASTM International, *ASTM E704 - Standard Test Method for Measuring Reaction Rates by Radioactivation of Uranium- 238*, West Conshohocken, PA (2019).
6. ASTM International, *ASTM E261 - Standard Practice for Determining Neutron Fluence, Fluence Rate, and Spectra by Radioactivation Techniques*, West Conshohocken, PA (2021).
7. ASTM International, *ASTM E262 - Standard Test Method for Determining Thermal Neutron Reaction Rates and Thermal Neutron Fluence Rates by Radioactivation Techniques*, West Conshohocken, PA (2017).
8. ASTM International, *ASTM E181 - Standard Guide for Detector Calibration and Analysis of Radionuclides in Radiation Metrology for Reactor Dosimetry*, West Conshohocken, PA (2023).
9. ASTM International, *ASTM E944 - Application of Neutron Spectrum Adjustment Methods in Reactor Surveillance*, West Conshohocken, PA (2019).
10. L.R. Greenwood and C.D. Johnson, *User Guide for the STAYSL PNNL Suite of Software Tools*, PNNL-22253, Pacific Northwest National Laboratory. Richland, WA (USA), Pacific Northwest National Laboratory. Richland, WA (USA) (2013).
11. P.J. Griffin, J.G. Kelly, and J.W. VanDenburg, *User`s manual for SNL-SAND-II code*, Sandia National Labs., Albuquerque, NM (USA), (1994).
12. P.L. Mulligan, B.A. La Riviere, and D.C. Glasgow, *Modeling and Design of Micro Flux Monitors for Neutron Fluence Measurements* ORNL/TM-2024/3345, Oak Ridge National Laboratory, Oak Ridge, TN (2024).
13. R.D. Cheverton and T.M. Sims, *HFIR Core Nuclear Design*, ORNL-4621, Oak Ridge National Laboratory, Oak Ridge, TN (1971).